Clean Nanotube Unzipping by Abrupt Thermal Expansion of Molecular Nitrogen: Graphene Nanoribbons with Atomically Smooth Edges

Aarón Morelos-Gómez,[†] Sofia Magdalena Vega-Díaz,[‡] Viviana Jehová González,[§,#] Ferdinando Tristán-López,[‡] Rodolfo Cruz-Silva,[‡] Kazunori Fujisawa,[†] Hiroyuki Muramatsu,[†] Takuya Hayashi,[†] Xi Mi,[∥] Yunfeng Shi,[∥] Hirotoshi Sakamoto,[‡] Fitri Khoerunnisa,[‡] Katsumi Kaneko,[‡] Bobby G. Sumpter,[⊥] Yoong Ahm Kim,[†] Vincent Meunier,[∥,¶] Morinobu Endo,[†,‡] Emilio Muñoz-Sandoval,[▲,#] and Mauricio Terrones[‡,▽,*]

[†]Faculty of Engineering and [‡]Research Center for Exotic Nanocarbons (JST), Shinshu University, 4-17-1 Wakasato, Nagano 380-853, Japan, [§]Departamento de Ciencia e Ingeniería de Materiales e Ingeniería Química, Universidad Carlos III, Av. Universidad 30, 28911 Leganés, Madrid, Spain, [⊥]Center for Nanophase Materials Sciences and Computer Science & Mathematics Division, Oak Ridge National Laboratory, P.O. Box 2008, MS6367, Oak Ridge, Tennessee 37831-6367, United States, [∥]Department of Materials Science and Engineering and [¶]Department of Physics, Applied Physics, and Astronomy, Rensselaer Polytechnic Institute, 110 Eighth Street, Troy, New York 12180-3590, United States, [▲]Instituto de Microelectrónica de Madrid, IMM (CNM-CSIC), Newton 8, Tres Cantos, Spain, and [▽]Departments of Physics and of Materials Science and Engineering and Materials Research Institute, The Pennsylvania State University, 104 Davey Lab, University Park, Pennsylvania 16802, United States. [#]On leave from the Advanced Materials Department, Instituto Potosino de Investigación Científica y Tecnológica, A.C., Camino a la Presa San José 2055, Col. Lomas 4a. sección, San Luis Potosí, SLP 78216, México.

ABSTRACT We report a novel physicochemical route to produce highly crystalline nitrogen-doped graphene nanoribbons. The technique consists of an abrupt N_2 gas expansion within the hollow core of nitrogen-doped multiwalled carbon nanotubes (CN_x-MWNTs) when exposed to a fast thermal shock. The multiwalled nanotube unzipping mechanism is rationalized using molecular dynamics and density functional theory simulations, which highlight the importance of open-ended nanotubes in promoting the efficient introduction of N_2 molecules by capillary action within tubes and surface defects, thus triggering an efficient and atomically smooth unzipping. The so-produced nanoribbons could be few-layered (from graphene bilayer onward) and could exhibit both crystalline zigzag and armchair edges. In contrast to methods developed previously, our technique presents various advantages: (1) the tubes are not heavily oxidized; (2) the method yields sharp atomic edges within the resulting nanoribbons; (3) the technique could be scaled up for the bulk production of crystalline nanoribbons from available MWNT sources; and (4) this route could eventually be used to unzip other types of carbon nanotubes or intercalated layered materials such as BN, MoS_2, WS_2, *etc.*

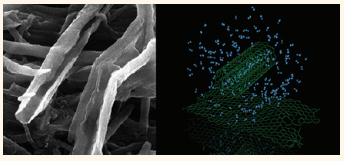

KEYWORDS: carbon nanoribbon · carbon nanotube · molecular expansion · nitrogen-doped · unzipping

The discovery of graphene and, subsequently, graphene nanoribbons (GNRs) has set a new dimension for nanoscale carbon science. Graphene exhibits its extraordinary electrical,[1] thermal,[2] and mechanical properties[3] and can potentially lead to numerous applications in electronic devices, sensors, and composites.[4,5] GNRs have been synthesized using a number of methods, including mechanical cleavage followed by lithography, etching, and chemical stripping.[4−7] However, other methodologies such as chemical vapor deposition (CVD) have been successfully carried out to produce bulk quantities of graphitic nanoribbons.[8] A common drawback of these methods is the formation of "rough" or imperfect edges within the nanoribbons. These rough edges significantly affect the electronic properties and chemical activity of the nanoribbons, and to the best of our knowledge, methods able to obtain bulk quantities of nanoribbons exhibiting atomically sharp edges have not been reported hitherto. In this work, we report a novel and facile method for synthesizing few-layer N-doped GNRs, using nitrogen-doped multiwalled carbon nanotubes (CN_x-MWNTs) as starting material, based on an abrupt unzipping[9] *via* the thermal expansion of N_2 molecules inserted in surface defects and in the hollow core of the concentric tubes. The presence of limited amount of structural defects (*e.g.*, uncapped tubes, pyridine-like sites, and large vacancies) is found to facilitate the diffusion of liquid N_2 into the tubes' cores and within their external concentric cylinders, thus promoting an atomically smooth CNT unzipping.

The unzipping of carbon nanotubes using strong chemical treatments has been recently reported. In this context, Tour and

* Address correspondence to mut11@psu.edu, mtterrones@shinshu-u.ac.jp.

Received for review November 8, 2011 and accepted February 23, 2012.

Published online February 23, 2012
10.1021/nn2043252

co-workers used a strong chemical route based on sulfuric acid (H_2SO_4), potassium permanganate ($KMnO_4$), and heating, in order to open up nanotubes longitudinally.[10] Similarly, Cano-Márquez *et al.* have unzipped chemically shortened CNTs by the intercalation of lithium (Li) and ammonia (NH_3).[11] However, in both cases, the resulting graphitic nanoribbons are relatively wide and do not exhibit atomically smooth edges since the severe acid treatments required in these techniques damage the edges due to heavy chemical functionalization, thus affecting their electronic properties. Dai's group has developed a technique able to create very narrow graphene nanoribbons (<10 nm). In this multistep process, arc-grown MWNTs are partially embedded in a polymer film and are etched with gas plasma. Subsequently, the film is removed using solvent vapor followed by heat treatment of the resulting nanoribbons in order to remove any residue.[12] More recently, Datta *et al.*,[13] Ci *et al.*,[14] and Elías *et al.*[7] independently demonstrated the controlled catalytic cutting of graphite substrates and the unzipping of carbon nanotubes when metal nanoparticles were deposited on these substrates and -were subsequently heated to 800−900 °C in the presence of H_2; the process has been addressed in the literature as catalytic hydrogenation of carbon.[7] Kim and co-workers designed an alternative method to produce GNRs from multiwalled carbon nanotubes (MWNTs), performed under high vacuum, in a non-chemical environment. Electrical current and nanomanipulation was used to unwrap a portion of the MWNT and thus produce GNRs of specific widths and lengths.[15]

Unfortunately, only very few methods have been developed to produce atomically smooth edges within GNRs. Some of these methods apply a bottom-up approach by intermolecular coupling of monomers that results in nanoribbons of several nanometers in length.[16] Other methods have used the top-bottom approach *via* sonication of mildly oxidized arc produced MWNTs[17,18] and the hydrogenation of SWNTs.[19] However, these methods have reported low yield of nanoribbons from the starting material, involve non-facile or time-consuming procedures, and may require expensive reacting agents. In addition, most of the previous methods used to unzip nanotubes result in a high content of structural defects and large volumes of chemical waste products caused by the strong acid treatments. Therefore, alternative routes to produce large quantities of graphene nanoribbons with atomically sharp edges need to be implemented. In contrast, the method presented here uses nanotubes grown by chemical vapor deposition (CVD) and is able to produce large quantities of GNRs where many of them exhibit crystalline edges using inexpensive materials such as MWNTs (N-doped), liquid nitrogen, and boiling water. More importantly, the process does not form graphene oxide (GO) waste products obtained by strong acid treatments. Our method consists of an abrupt expansion of encapsulated molecular nitrogen in MWNTs, which triggers an atomically smooth unzipping of carbon nanotubes.

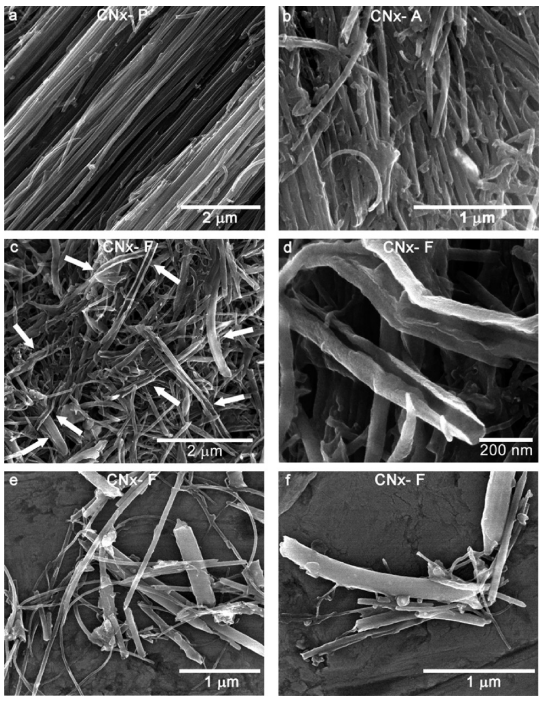

Figure 1. SEM images of unzipped CN_x-MWNTs. SEM images of (a) pristine (CN_x-P); (b) acid-treated (CN_x-A); (c−f) unzipped CN_x-MWNTs (CN_x-F); arrows indicate unzipped CN_x-MWNTs. (c) Low magnification of CN_x-F sample showing several unzipped carbon nanotubes, (d) curved CN_x-NRs, and (e,f) flat CN_x-NRs.

RESULTS AND DISCUSSION

Figure 1a depicts an SEM image of pristine CN_x-MWNTs (CN_x-P), and Figure 1b shows mild acid-treated CN_x-MWNTs (CN_x-A) exhibiting open nanotube ends that would allow the facile introduction and diffusion of liquid N_2. Subsequently, the CN_x-A samples impregnated with liquid N_2 and exposed to the thermal shock in boiling water reveal an efficient unzipping (see Figure 1c−f); the sample is labeled as CN_x-F. In addition, the sample was reduced by heating in Ar at 1000 °C and labeled as CNx-FHT; this sample will be discussed below. We identified three types of unzipped structures: (a) partially unzipped CN_x-MWNTs exhibiting a "V-shape",[10,11,20] (b) curved nanoribbons, and (c) completely flat CN_x nanoribbons. Approximately 1400 structures were identified by SEM, and 54% of the structures corresponded to closed CN_x-MWNTs, whereas 46% were unzipped. From the unzipped structures, we determined that 11% were partially unzipped V-shape tubes, 53% were curved nanoribbons, and 36% consisted of completely flat nanoribbons. The average diameter of the pristine CN_x-P was 64 ± 10 nm, and the average width of the

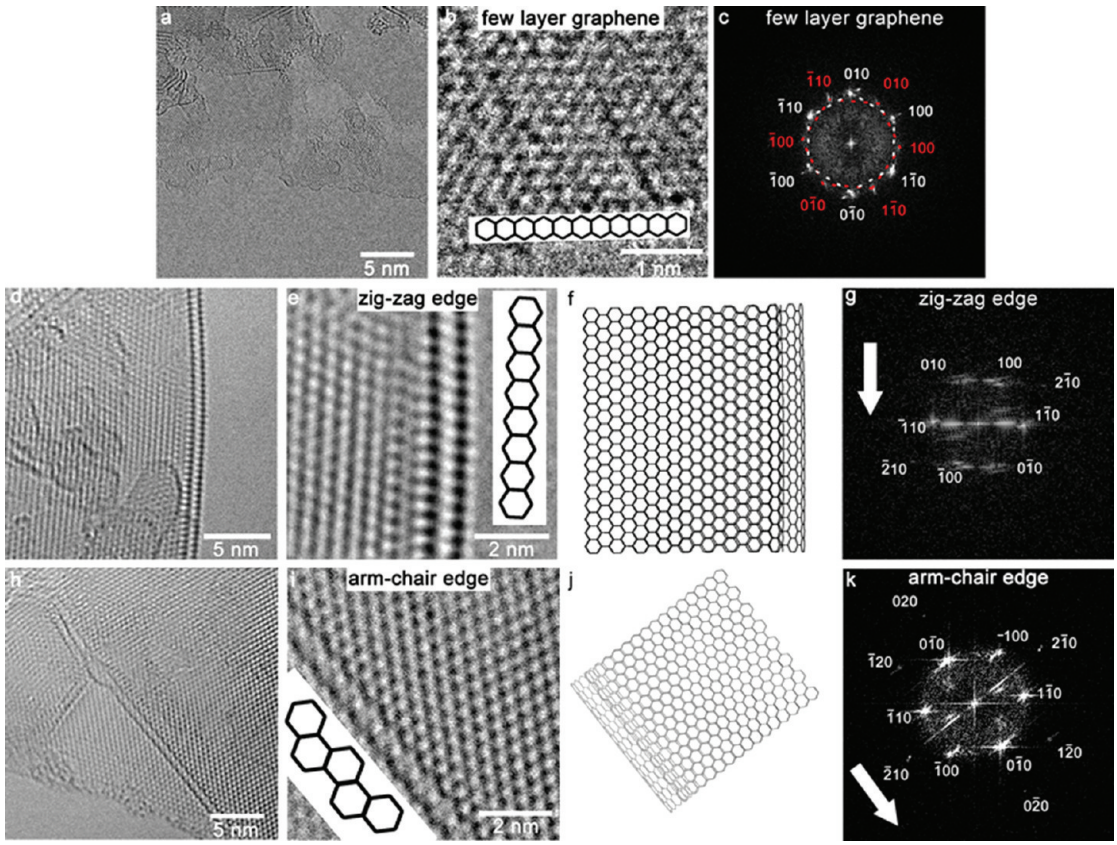

Figure 2. HRTEM images and fast Fourier transformation of unzipped CN_x-MWNTs. (Left and middle) HRTEM images and (right) their corresponding fast Fourier transformations (FFT) of unzipped CN_x-MWNTs. (a−c) Rotated layer stacking of the CN_x-NRs, (d−g) zigzag, and (h−k) armchair edges of few-layered CN_x-NRs. Models of the nanoribbon (f) zigzag and (j) armchair edge. The images reveal the presence of atomically smooth edges (b,d,e,h,i); the parallel lines are due to the loop formation. The arrows indicate the edge direction of the nanoribbons.

carbon nanoribbons obtained after the thermal shock was 162 ± 30 nm. This size is relatively lower than expected for an unfolded nanotube, possibly due to loss of the outer walls during the acid treatment and the N_2 thermal expansion. The observed graphene nanoribbons appeared transparent in TEM with the absence of a hollow core, a common characteristic of carbon nanotubes, thereby confirming that some CN_x-MWNTs were completely unzipped and were effectively transformed into nanoribbons (see Figure 2a,d, h). Interestingly, HRTEM images reveal that the edges of these few-layer GNRs exhibited atomically smooth edges (see Figure 2 and Figure SI-1 in Supporting Information), and in some cases, the edges displayed a rotation of the hexagonal pattern caused by two layers (or set of layers) stacked with one another with a specific angle, as indicated by the fast Fourier transform (FFT; see Figure 2,bc). The flat CN_x-NRs exhibited atomically smooth and continuous edges corresponding to either zigzag or armchair terminations with ABAB... stacking within these few layers (see Figure 2e,i). These atomic edges exhibit lengths ranging between 10 and 60 nm (see Figure 2d,h and Figure SI-1), with fragments ranging between 15 and 55 nm long of irregular edges. In addition, we found that some of the edges loop at the ends, displaying zigzag or armchair termination (see Figure SI-1jo); these are folded layers creating loops on the edge, and these edges appear darker due to the overlap of carbon atoms. From the observed structures, 58% exhibit zigzag and 38% exhibit armchair terminations and 4% are chiral. It is noteworthy that these continuous edges have mainly been observed in CVD-grown graphitic nanoribbons that were Joule-heated/irradiated under a HRTEM,[8,21,22] and to the best of our knowledge, such continuous edges have not been previously observed in chemically treated nanotubes produced by CVD. We attribute this result to the abrupt expansion of liquid N_2, which resulted in the uniform (or atomically smooth) breakage of the concentric nanotubes forming the MWNTs.

A dispersion of CN_x-F was also analyzed by scanning probe microscopy (SPM) in the dynamic force mode (DFM). We carried out DFM topography in order to obtain a better understanding of the shape and dimensions of the produced nanoribbons (*see* Figure 3). Figure 3a−c epicts the DFM topography of CN_x-MWNTs and CN_x-NRs. A curved V-shape nanoribbon of *ca.* 200 nm wide is observed in Figure 3a−c. From the surface profiles across the curved CN_x nanoribbons,

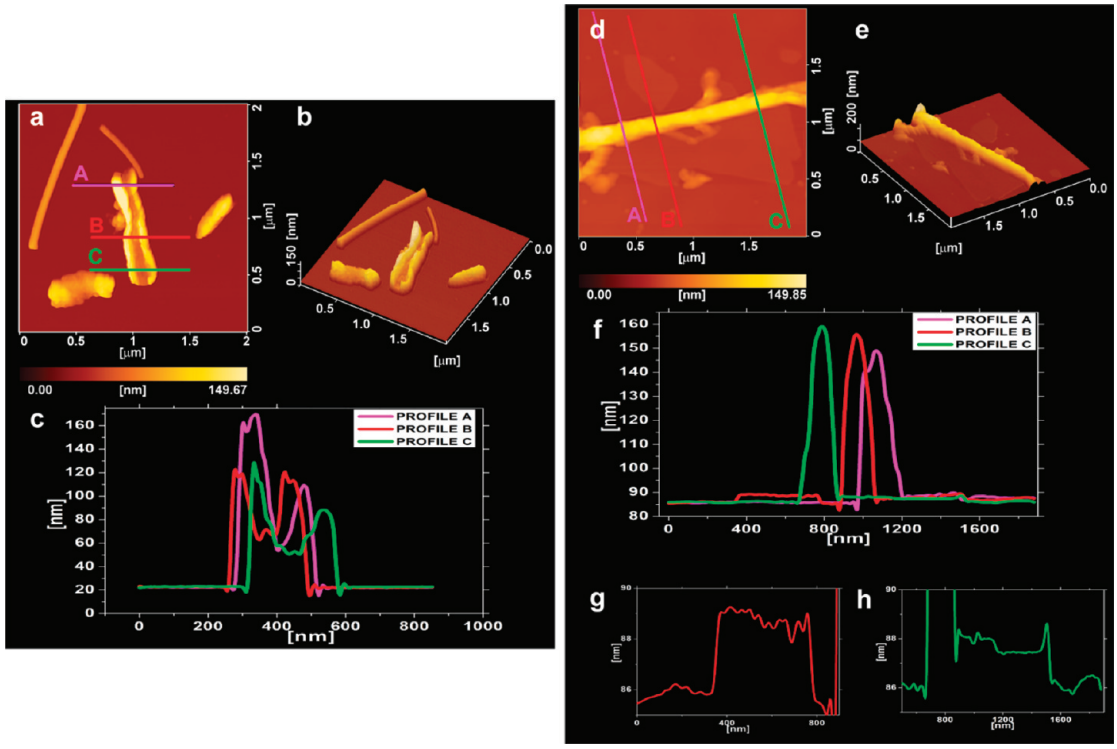

Figure 3. DFM analysis of unzipped CN_x-MWNTs. (a−c) Mixture of CNT, curved, and flat CN_x nanoribbons and (d−h) partially unfolded CN_x-MWNTs. (a,d) Topography, (b,e) 3-D topography, and (c,f,g,h) line profile showing the lines scans of different regions of the nanoribbons. (f,g,h) Line profile of an unfolded outer wall of a CN_x-MWNT with a smooth and flat sheet with a height of *ca.* 2−3 nm.

we could detect the different unzipped morphologies: V-shape (Figure 3a−c), flat-shape (Figure SI-2a−c), and flat/curved-shape (Figure SI-2d−f). In some cases, we observed amorphous-like nanoribbon segments that are flat and could be due to a high surface reactivity of CN_x with sulfuric acid and nitric acid creating a large number of vacancies within the structure (see Figure SI-2a−c). A partially unzipped CN_x-MWNT was observed in Figure 3d,e. Here, it appears that the outer walls were successfully unzipped, exhibiting a smooth and thin layered structure with a height of *ca.* 1−3 nm, corresponding to 2−5 layers of graphene (see Figure 3f−h). From our DFM observations, we found that the nanoribbon thickness is on the order of tens of nanometers corresponding to several layers; however, Figure 3d−h exhibits a thin few-layered structure.

The X-ray powder diffraction patterns of CN_x-MWNTs during the different stages of the process (Figure SI-3a in Supporting Information) reveal that the materials preserve a layered structure; however, the (002) planes start to broaden because the number of stacked layers is reduced after the formation of ribbons (fewer layers are perfectly stacked in the ribbon materials). We also noted extremely large interlayer distances after the acid treatment (CN_x-A), up to 9.3 Å (2θ located at *ca.* 10°). This large spacing is preserved, but in a reduced amount, after the thermal shock in boiling water possibly caused by the remaining presence of partially unzipped carbon nanotubes (see Figure SI-3a and Table SI-1 in Supporting Information). In the CN_x-A sample, we also noted other interlayer distances corresponding to 7.1 and 3.6 Å. Surprisingly, we also found another sharp reflection located at 3.1 Å (see Figure SI-3a), which corresponds to one-third of the 9.3 Å interlayer distance. The 3.1 Å interlayer distance has been observed previously in acid intercalated graphite.[23] It is noteworthy that the intercalation of graphite materials with sulfuric and nitric acid has been reported previously with interlayer distances up to 14 Å.[23−25] Possibly, the interlayer spacing observed in our samples (*ca.* 9.3, 7.1, and 3.1 Å) corresponds to a periodic intercalation of sulfuric acid that takes place within the outer walls of the MWNTs, similarly to the work of Shih *et al.*[26] and Chen *et al.*,[27] known as the staging phenomena,[28] in which there is an intercalation every two or three layers. This periodic intercalation may explain the 9.3 Å interlayer spacing as a reflection from the 3.1 Å. In addition, we observed that the intensity of the intercalation peaks of the unzipped CN_x-MWNTs (CN_x-F) is lower than that of the acid-treated CN_x-A (see Figure SI-3a). This observation indicates that, after the abrupt N_2 expansion, the signals originating from the acid intercalation decrease due to the formation of nanoribbons. It is believed that the few-layered unzipped tubes (*ca.* 50%) still contain intercalated acid, thus explaining the remaining intercalation peaks witnessed by X-ray powder diffraction. We believe that this acid intercalation facilitates

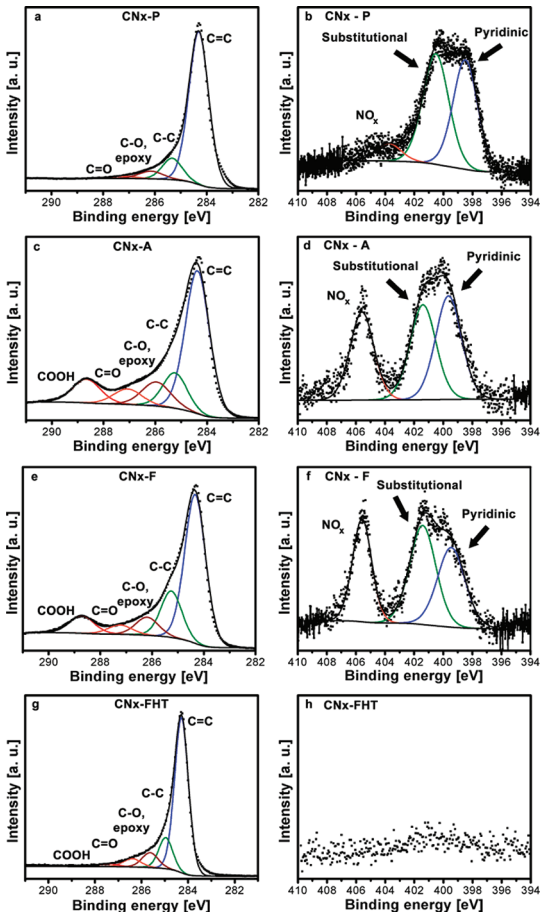

Figure 4. X-ray photoelectron spectroscopy of unzipped CN_x-MWNTs. (a,b) Pristine (CN_x-P), (c,d) acid-treated (CN_x-A), (e,f) unzipped (CN_x-F), and (g,h) heat-treated nanoribbons (CN_x-FHT). The C1s region is depicted in the left column, whereas the N1s binding energy appears in the right-hand column.

improved diffusion of N_2 molecules between the outer layers (see below calculations section), thus favoring the unzipping process. The presence of iron carbide (Fe_3C) during all stages of the process is expected since not all of the CN_x nanotubes are completely uncapped, and some of the carbide filling still remains inside partially unzipped nanotubes. Raman spectroscopy indicates that all of the N-doped samples exhibit the D band (*ca.* 1554 cm^{-1} and caused by the symmetry breaking of the hexagonal network induced by N doping), G band (*ca.* 1583 cm^{-1}), and G′ band (*ca.* 2650 cm^{-1}), and a shoulder next to the G band arises in the CN_x-F sample and corresponds to the D′ band (see Figure SI-3b). This D′ band at 1620 cm^{-1} in the Raman spectrum of the CN_x-F sample could originate from a large amount of edge sites, indicating the formation of nanoribbons through the effective exfoliation of MWNTs; furthermore, this peak becomes more evident with the 785 nm laser line (see Figure SI-3c). The disorder (edge formation, N-doping, and functional groups) increases during each stage of our method, shown by the variation in the I_D/I_G ratio (the integrated intensity of the D band divided by the integrated intensity of the G band) from 0.94 to 1.28. However, after the thermal treatment (CN_x-FHT), I_D/I_G remains practically unchanged (1.26) possibly due to the presence of the reactive bare edges of the ribbons (see Table SI-1 in Supporting Information).

XPS measurements were carried out in order to determine the chemical surface composition of the samples after each stage of our process, and such measurements provide insightful information regarding the binding energies of carbon compounds (see Figure 4). The carbon C1s peak exhibits the presence of sp^2- and sp^3-hybridized carbon (284.3 and 285.1 eV, respectively).[29,30] The sp^2 bonding content is reduced after the acid treatment from 37 to 30%. However, when the samples were unzipped (CN_x-F), the sp^2 content increased up to 45%, demonstrating that some amorphous-like carbon was removed and the produced nanoribbons are crystalline (see Table SI-2 in Supporting Information). In addition, the shoulder next to the sp^2-hybridized carbon observed after acid treatment is increased and reveals the presence of various C−O compounds, such as C−O/epoxy, carbonyl, and carboxyl groups (286.4, 288.7, and 290.9 eV, respectively).[30,31] We thus suggest that the area of the carboxyl groups attached to the highly defective sites of the carbon nanotubes and to the edges of the nanoribbons increases. The carbon to oxygen ratios (C/O) correspond to 48, 3.9, 4.2, and 10.1 for CN_x-P, CN_x-A, CN_x-F, and CN_x-FHT, respectively. The observed decrease in C/O ratio is mainly due to an edge oxidation process (oxygenated groups adsorbed on the surface), first by removing the tube ends (CN_x-A), and then by unzipping them into ribbons (CN_x-F). It is noteworthy that the content of oxygen functionalities observed for these nanoribbons (see Figure 4e and Table SI-2) is not as high as those shown for graphene oxide and graphene oxide nanoribbons.[32−34] Regarding the N1s region, we found several changes at each stage of the unzipping process (see Figure 4): (1) The content of substitutional nitrogen (N bonded to three carbon atoms) to pyridinic nitrogen (N bonded to two carbon atoms) varies 2, 0.5, and 1.15 for CN_x-P, CN_x-A, and CN_x-F, respectively; the observed increase in pyridinic sites could be caused by the presence of nitrogenated molecules along the edges within the nanoribbons. (2) There is an increase of NO_x within the samples, which is caused by the adsorption or intercalation of nitric acid in the CN_x-F sample; such intercalation has been observed by other authors[24,25] and our XRD patterns confirm this scenario (see Figure SI-3a). (3) The overall nitrogen content from the XPS suface analysis demonstrates a small decrease from 2 to 1 atom %, possibly caused by the lower content of pyridine-like nitrogen sites (at least by a 30% reduction; see Table SI-2 in Supporting Information). These sites are thought to be more reactive and appear to be

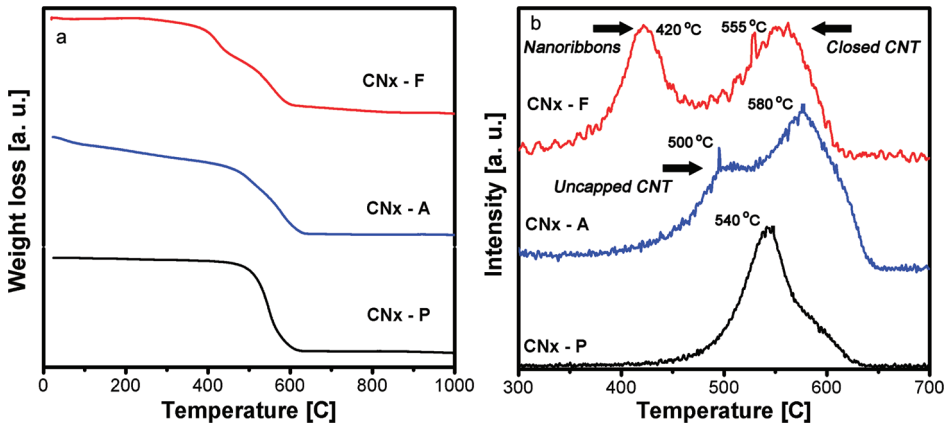

Figure 5. Thermogravimetric analysis of unzipped CN_x-MWNTs. (a) TGA of the different samples and (b) derivative of the weight loss *vs* temperature. The analysis was carried out using 1 mg of sample in air at a heating rate of 10 °C/min. The results clearly indicate the presence of two kinds of materials within samples CN_x-A and CN_x-F.

key for enhancing the unzipping propagation. According to XRD and XPS studies, it is important to emphasize that our unzipped nanotubes do not show the formation of GO and exhibit a higher degree of crystallinity when compared to previously reported GNRs obtained by unzipping CVD-grown carbon nanotubes.

We carried out thermogravimetric analysis (TGA) in atmospheric conditions to have a better understanding about the chemical reactivity of the nanoribbon materials (see Figure 5). The TGA plots (see Figure 5a) indicate that the samples possess different thermal decomposition temperatures. The derivative of TGA (DTGA) of CN_x-P exhibits one single peak centered at 540 °C. However, CN_x-A exhibits two peaks: one located at 500 °C and another at 580 °C. This shows that there are two kinds of reactive materials within the sample; open-ended tubes and the remaining closed CN_x-MWNTs (see Figure 5b). The acid treatment used in our study may also clean the sample, retaining the most stable crystalline structures, therefore increasing the thermal stability of the entire analyzed sample. Furthermore, the CN_x-F sample clearly shows two independent peaks located at 420 and 555 °C. This first peak may correspond to the CN_x-NRs that contained edges that yield to higher reactivity, and the following peak centered at 555 °C corresponds to the CN_x-MWNTs that were not fully unzipped. To understand better the intercalation of acid within the MWNTs, we carried thermogravimetric mass spectrometry measurements of the CN_x-P, CN_x-A, and CN_x-F samples (see Figure SI-4) with a flow of He/O_2. The CN_x-P sample exhibits the release of C (m/z = 12), CO (m/z = 12), and CO_2 (m/z = 44), corresponding to the decomposition of the carbon nanotubes, without any signal of SO_3 (m/z = 64). The acid-treated sample (CN_x-A) exhibits the release of SO_3 at two temperatures; we attribute the first release at *ca.* 325 °C to sulfuric acid physisorbed on the surface of the MWNTs, where it would decompose into SO_3 and H_2O, and the second peak at *ca.* 625 °C corresponds to SO_2 and SO_3 intercalated within the outer walls of the MWNTs; once SO_2 is released, it would react with oxygen in the atmosphere and transform into SO_3. The second peak of SO_3 corresponds with the release of C, CO, and CO_2, showing that, due to the decomposition of the outer walls of the MWNTs, the SO_x intercalated species are released. The CN_x-NRs exhibit a small shoulder at *ca.* 350 °C, and this is smaller than the CN_x-A sample due to a washing effect from the exposition to hot water. The peak located at *ca.* 575 °C arises from MWNTs that were not unzipped. C, CO, and CO_2 exhibit a small peak around 440 °C due to the decomposition of the edges of the NRs, and the second peak at *ca.* 560 °C is due to the MWNTs that are not unzipped, as previously discussed.

Our nitrogen adsorption isotherms show that the adsorption and desorption branches are very similar, with a small deviation of the desorption branch starting at 0.7 and 0.5 P/P_o for the acid-treated (CN_x-A) and nanoribbon (CN_x-F) samples (see Figure SI-5a). When carefully observing the plots, we found that the acid-treated sample exhibits an upward deviation which we attribute to capillary condensation,[35,36] where nitrogen infiltrates the hollow inner cores of the MWNTs through the open ends or large vacancies located on the surface of the tubes. For nanoribbons (CN_x-F), we found that they exhibit a higher adsorption throughout all of the measured pressures when compared to the pristine sample (see Figure SI-5b,c). We attribute this phenomenon to a higher interaction of the gas with exposed edges of the nanoribbons. From our adsorption measurements, we found that the BET surface areas are 32.9, 6.8, and 45.7 m^2/g for CN_x-P, CN_x-A, and CN_x-F, respectively. The measurements were carried out for flakes (CN_x-P) and buckypaper of our samples (CN_x-A and CN_x-F). It is clear that our acid-treated sample exhibits a lower surface area due to its more compact nature.[37] However, our nanoribbon samples exhibit a higher surface area due to unzipping

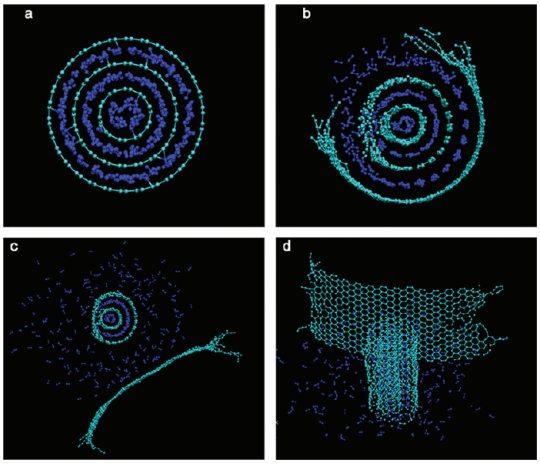

Figure 6. Molecular dynamics simulation of the unzipping process. Different frames of the MD simulations considering a triple-walled armchair carbon nanotubes filled with N_2 molecules heated at 1500 K. (a) N_2 intercalated in the multiwalled carbon nanotube, (b) thermal expansion of N_2 and the subsequent unzipping of the outer shell, (c) release of N_2 and detachment of the outer wall forming a graphene nanoribbon, and (d) isolated carbon nanoribbon and a double-walled carbon nanotube filled with N_2.

of the nanotubes which result in exposed and atomically smooth edges.

When comparing our unzipped MWNTs with graphene oxide (GO), we observe clear differences between both materials in our characterization studies. From SEM, TEM, and AFM images (see Figure 1, Figure 2, Figure 3, Figures SI-1 and SI-2), we did not find as many single-, bi-, and few-layer structures as in GO.[32] In addition, our XPS spectra show that acid treatment creates oxidation on our MWNTs; however, the intensity and width of the oxidation peaks show that the oxygen functionality content is much lower when compared to GO.[32−37] Our X-ray diffraction patterns (see Figure SI-3a) reveal large spacings similar to those observed for GO; nevertheless, we believe that in our case it is due to intercalation of acid and not graphene oxide production, as previously discussed. For these reasons, we find that our nanoribbons resemble neither the chemical structure nor morphology of graphene oxide.

In order to elucidate the unzipping mechanism, triggered by the abrupt expansion of the trapped molecular N_2 within the CN_x-MWNTs, we have carried out large-scale molecular dynamics (MD) simulations of the complete process, consisting of expanding N_2 gas inside the open nanotubes. The carbon−carbon interaction is treated using adaptive intermolecular reactive bond order (AIREBO) potential,[38] which can accurately describe both intramolecular bond breaking/formation and intermolecular dispersion forces. The nitrogen−nitrogen and nitrogen−carbon interaction are adopted from ref 39. In this model, N_2 molecules do not dissociate, and it is therefore well suited to the modeling of N_2 liquid expansion. The intramolecular force for nitrogen atoms within a diatomic molecule is a harmonic spring $\phi_{harmonic}(r) = 1/2K(r - r_{eq})^2$ with a spring constant K of 22.95 N/cm, and an equilibrium spring length r_{eq} of 1.10 Å. N_2-N_2 and N_2-C interactions are in the form of standard Lennard-Jones potential $\phi_{LJ}(r_{ij}) = 4\varepsilon[(\sigma/r_{ij})^{1/2} - (\sigma/r_{ij})^6]$. The energy scale ε is 0.00314 and 0.00288 eV for N_2-N_2 and N_2-C, respectively. The length scale σ is 3.32 and 3.36 Å for N_2-N_2 and N_2-C, respectively.

Both armchair ((5,5)@(10,10)@(15,15)) and zigzag ((9,0)@(18,0)@(27,0)) triple-walled nanotubes were constructed with N = 1560 (L = 31.97A) and N = 2160 (L = 42.00A) carbon atoms in separate simulations. Molecular nitrogen was inserted inside the tubes at liquid nitrogen densities (0.034 N_2/A^3), corresponding to 328 and 473 nitrogen molecules added into the armchair and zigzag systems, respectively. Periodic boundary conditions were employed along the length of the nanotubes (see Figure 6a). The systems were quickly heated to 1500 K in order to simulate the thermal shock. The simulation system is coupled to a Nose-Hoover thermostat in order to maintain a high temperature of 1500 K. A small time step of 0.1 fs is used to ensure integration stability at such a high temperature. Initially, the entire system is found to expand quasi-uniformly in a breathing-like fashion (see Figure 6a) in order to accommodate the expanded gaseous N_2 (see MD animation 1 in the Supporting Information). The system remains in this metastable form for a certain amount of time until fluctuations in the atomic positions on the outer wall eventually break the symmetry, thus resulting in a sharp increase in the local stress which then forms defective carbon rings (*e.g.*, vacancies, octagons, pentagon−heptagon pairs, depending on the run). These defects act as nucleation sites, and the tube is readily unzipped along a line quasi-parallel to the tube axis (see Figure 6b). Note that the inner tubes remain unaltered, probably because of their higher curvature and stiffness (see Figure 6c). In addition, when the same simulation is performed with only the outer shells (not shown here), we did not observe any unzipping, as the stress caused by thermal shock is accommodated by the correlated motion of N_2 inside the large cavity inside the tube. To further demonstrate the importance of local stress, we repeated the calculations for the zigzag tube by initially including 5775 (pentagon, heptagon, heptagon, pentagon) defects (two configurations were considered separately; see Figure SI-6 and MD animation 2 in the Supporting Information). We found that the presence of these topological 5775 defects facilitates the unzipping, which initiates at the defect position. In each simulated case, the resulting GNRs show a number of defects on the edges (most notably carbon chain, a known product of the AIREBO potential; see Figure 6d), while the basal planes are found to be remarkably well-ordered. When the MD is carried out

further, the nanoribbon is fully detached from the multiwalled nanotube (see Figure 6d). Quite interestingly, the absence of a substrate in these calculations leads to the formation of nanoribbon loops (not shown here), an observation that is in agreement with several experimental findings. Movies related to the MD calculations depicting the unzipping caused by the rapid expansion of N_2-trapped in different types of triple-walled carbon nanotubes (armchair type, zigzag type, and defective structures) can be viewed in the Supporting Information.

It is also important to emphasize that MD calculations with N_2 molecules only inserted inside the innermost tube have not shown unzipping. It is therefore possible that the mechanism requires the partial insertion (diffusion) of N_2 molecules on the outer walls close to pore defects (large vacancies), as well as the full filling of N_2 molecules inside the innermost tube (inner core). In this context, we carried out DFT/LDA (see SI for details) calculations for the insertion of a single N_2 molecule into a triple-layer CNT. The energy values are depicted in Table SI-3. These calculations were obtained based on gamma point DFT/LDA calculations using PAW with a 400 eV cutoff (full relaxation). The associated insertion energy into the inner tube is negative/attractive as showm in the BET measurements, -0.22 eV (very easy to fill the inner cores of opened tubes), while intercalation of the first layer is $+3.42$ eV and the outer layer is $+1.64$ eV. We noted that intercalation significantly distorts the tube walls with a larger change for the other tube case giving an interlayer distance of 5.1 Å *versus* the first layer interlayer distance of 3.72 Å. That is why the intercalation energy is less on the outside. This value is close to the 3.6 Å observed experimentally and explains why we usually observe the unzipping of the outer layers first (see Figure 3d,e). Although this intercalation energy is still relatively large, we should note that these calculations were carried out using pristine tubes (defect-free), and one should expect smaller values for tubes that have defects or partial acid intercalation. For example, we have found that having a nitrogen substitutional defect on the tube wall lowers the intercalation energy from 1.64 to 1.53 eV. Additionally, we examined the intercalation of different chemical species (N_2, SO_2, SO_3, S, and H) and MWCNT defects (nitrogen substitutional, pyridine (N3), vacancy, and epoxy), based on full ionic relaxation using the DFT/PBE functional with dispersion corrections and planewave PAW pseudopotentials with an energy cutoff of 400 eV (see Table SI-4). Nitrogen molecules intercalate better when two outer walls have defects (N3 pyridine, outer wall + vacancy next wall) than just the first outer wall (single N atom substituted CNT), with intercalation energies relative to pristine TWNTs of -0.99 and -0.59 eV, respectively. The intercalation energies of the SO_2 and SO_3 are lower for the epoxy defects, followed by the vacancy, N3 pyridine, and finally with single substitutional N (all defects are on the outer wall); in all of these cases, the SO_3 exhibits lower intercalation energies. The epoxy defects are great attractors for SO_2 and SO_3 (see Figure SI-7a,b) (especially for SO_3), with intercalation energies for the first outer layer of $+0.93$ and -2.18 eV, respectively, and intercalation energies relative to the pristine triple-walled nanotubes (TWNTs) of -0.43 and -3.51 eV, respectively. The charge distribution of SO_3 within the TWNTs with an epoxy defect on the outer wall shows a high interaction between carbon from the outer wall and sulfur from SO_3 (see Figure SI-7c); this is not observed for the case of SO_2.

The experimental and theoretical evidence allows us to devise a model of the thermal shock unzipping mechanism. CN_x-MWNTs are found to unzip into GNRs due to the abrupt expansion of molecular N_2. While pure nanotubes are relatively chemically inert, they do not possess a large number of structural defects (*e.g.*, vacancies, dopants, adatoms, 5775 defects). However, strong and mild acid treatments have been used to uncap, exfoliate, or unzip carbon nanotubes, carbon fibers, and graphite,[9,10,23−25] and in this case, acid treatment is used to uncap the nanotubes. In some cases, the acid is intercalated within the graphitic planes.[23−25] Here, SO_2 and SO_3 from H_2SO_4 are interclated within the outer layers of the MWNTs, adding strain to the outer walls. When nitrogen molecules are then adsorbed by capillary condensation in the hollow cores of the uncapped acid-treated nanotubes (CN_x-A) and subjected rapidly to hot water, the nitrogen molecules rapidly expand as well as release gases from the intercalated acids, and the outer wall tube suffers a linear breakage that leads to the release of gaseous N_2 and SO_2 and SO_3 molecular species (see Figure 7). When nitrogen is not uniformly distributed within the tube, the method may create partially unzipped V-shaped CN_x-MWNTs, partially unfolded CN_x-MWNTs, and curved CN_x-NRs (see Figure 7). It is important to emphasize that experiments carried out without the abrupt expansion of N_2 only showed minute amounts of unzipped tubes (yields lower than 2−3%). We attribute this unzipping to the possible exfoliation of acid intercalated tubes triggered by sonication. In addition, experiments with abrupt heating with N_2 (made in a differential scanning calorimetry apparatus) and others heated rapidly in a furnace (1000 °C) with inert atmosphere did not give NRs. Also, repeating the abrupt expansion of liquid N_2 with hot water of CN_x oxidized in air did not yield NRs. The method presented here is a combined effect of the N_2 expansion with the intercalated SO_x species that apply strain to the outer walls; using water as a rapid heating and reactive medium, here the liberated SO_3 may react with water, forming H_2SO_4. Preliminary experiments with undoped

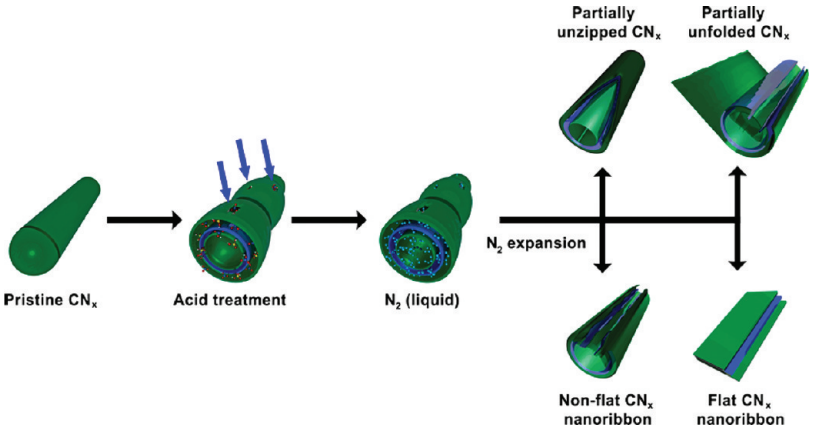

Figure 7. Proposed unzipping mechanism. Pristine CN_x-MWNTs with caps are treated with acid and are responsible for creating (blue arrows) small vacancies on the CN_x surface; the interlayer distances of the planes increase and liquid N_2 is then intercalated within the planes. After the liquid N_2-treated CN_x-A is subjected to hot water, N_2 expands abruptly, thus causing the CN_x-MWNTs to longitudinally unzip. From this process, it is possible to obtain partially unzipped CN_x-MWNTs, partially unfolded CN_x-MWNTs, nonflat CN_x nanoribbons, and flat CN_x nanoribbons.

MWNTs have shown similar results with nanoribbons exhibiting smooth edges.

Resistivity measurements at room temperature indicate resistivity values of 0.55, 0.89, 1.6, and 0.10 Ω·cm for CN_x-P, CN_x-A, CN_x-F, and CN_x-FHT, respectively (see Table SI-5 in the Supporting Information). The high resistivity in the CN_x-A and CN_x-F samples (Figure SI-8a) could be explained by the presence of bare edges and functional groups within the carbon nanotubes caused by the acid treatment and the thermal shock; however, these resistivity values are much lower values than those reported for graphene oxide.[32,40] Surprisingly, the heat-treated ribbon material (CN_x-FHT), reduced the oxygen functionality content (see Figure 4g and Table SI-2), revealing a clear decrease in electrical resistivity, 5 times lower than that of the pristine CN_x-MWNT sample. However, the annealed ribbons consist of conglomerated ribbons and planes that had experienced some morphological changes. We fitted our results using the variable range hopping (VRH) model for (a) Coulomb gap variable range hopping, (b) two dimensions (2D-VRH), and (c) three dimensions (3D-VRH) at temperatures below 50 K. In this model, resistivity values exhibit $T^{-1/2}$, $T^{-1/3}$, and $T^{-1/4}$ dependence for the three respective regimes.[41] We observed that CN_x-P follows a 2D-VRH behavior (see Figure SI-8c), in accordance with the conduction mechanism of disordered CNTs observed by other authors.[42] Here, the disorder may originate from nitrogen doping. The CN_x-A, CN_x-F, and CN_x-FHT behave as Coulomb gap VRH for temperatures ranging from 50 to 8 K, 50 to 5.5 K, and 50 to 2 K, respectively (see Figure SI-8b). This conduction mechanism has also been observed for disordered carbon nanoribbons.[43−45] The disorder may arise from the interplay between nitrogen doping, disordered nanoribbon edges, and functional groups, thus causing strong localization of electrons.[42,43,46,47] This strong localization resulting by the introduction of defects in semiconductors is known as Anderson localization.[48] The obtained activation energies at room temperature vary (see Table SI-5 in the Supporting Information). For temperatures above 300 K, we recorded values of 324, 7093, 11 250, and 274 meV for CN_x-P, CN_x-A, CN_x-F, and CN_x-FHT, respectively. The thermal treatment of the unzipped CN_x-F decreases the activation energy to a value lower than that of pristine CN_x-MWNTs. Other authors have reported activation energies ranging from 400 to 700 meV for amorphous carbon,[49] 200−1000 meV for nitrogen-doped amorphous carbon,[50] and 13−290 meV for carbon nanotubes.[51,52] The tendencies of the activation energies and the resistivities are similar, suggesting a modification of the electronic structure of the samples. At first, the values for the pristine samples are low in the range of nitrogen-doped amorphous carbon,[48] then the acid treatment introduces defects (intercalated species, vacancies, functional groups) increasing the activation energy; after the nanotubes are unzipped, the edges may have been functionalized requiring more energy for electron conductivity. Finally, when reducing the sample (lowering the amount of functional groups), the activation energy and the resistivity are lower than the pristine sample, and this suggests that the degree of functionalization heavily modifies the conductivity of NRs. From these results, one would expect that bulk samples of CN_x-F and CN_x-FHT may be excellent fillers for fabricating transparent and highly conducting substrates, in addition to robust composites or efficient nonmetal catalytic supports.

CONCLUSIONS

In summary, we have developed an efficient, inexpensive, and facile method capable of producing crystalline nitrogen-doped few-layer GNRs exhibiting atomically smooth edges. We found that this

mechanism (see Figure 7) is based on the following steps: (1) an acid treatment used to remove the nanotube caps and result in shortened the tubes; (2) a slight increase of the interlayer distance within the graphene cylinders caused by an acid treatment, so that N_2 molecules are easily inserted in the outer layers of the tubes; (3) the presence of some structural defects (*e.g.*, pyridine-like sites, vacancies, epoxy groups) within the outer layers of the tubes, facilitating the insertion of N_2 molecules and the unzipping propagation, and (4) intercalated SO_2 and SO_3 species situated at the defects (pyridine-like sites vacancies, epoxy groups) of the MWNTs within the outer walls inducing strain; (5) the abrupt expansion of the N_2 molecules and other inserted molecules (due to a abrupt temperature change) causing an atomically smooth unzipping of the MWNTs starting at the defect sites, thus creating highly crystalline nanoribbons as well as partially unzipped nanotubes. Our MD simulations confirmed that N_2 molecules need to be inserted within the hollow cores of the MWNTs, and that the presence of structural defects on the outer shells could help to accelerate this atomically smooth unzipping process. All of our characterization measurements confirm that the nanoribbons are mildly oxidized and exhibit a good degree of crystallinity; almost perfect zigzag and armchair edges were observed. In addition, the presence of bare edges makes our GNRs more reactive, as shown by TGA. We also found experimentally that the introduction of structural defects within the unzipped tubular structures (uncapped tubes, vacancies, and functional groups), caused by acid treatment, generates an Anderson-type strong localization at low temperatures (<50 K). We believe that this facile liquid N_2 method may be used for a variety of carbon nanostructures in order to exfoliate and unzip graphene and other intercalated layered materials such as BN, MoS_2, WS_2, and others.

METHODS

The synthesis of pristine CN_x-MWNTs (CN_x-P) was performed by chemical vapor deposition (CVD). The CVD was performed in an argon inert atmosphere carrying a aerosol solution, containing 5 wt % ferrocene ($FeCp_2$) with 95 wt % benzylamine (C_7H_9N), with a flow of 2.5 L/min at 825 °C.[53] The acid treatment was performed by adding 200 mg of CN_x-P in 30 mL of a solution of H_2SO_4/HNO_3 (3:1) and sonicated for 6 h. After sonication, the resulting solution was filtered and washed with deionized water and dried. Subsequently, the acid-treated CN_x-MWNT material (CN_x -A) was kept in a receptacle with liquid nitrogen for 5 min. The abrupt unzipping consists of adding boiling water to the recipient with CN_x-A and liquid nitrogen; here the temperature changed from *ca.* −200 to 45 °C between 5 and 10 s after adding boiling water. Further on, the dispersion was maintained under tip sonication at 80 °C for 30 min. These unzipped or exfoliated samples of CN_x-MWNTs are labeled as CN_x-F. Thermal treatment of the CN_x-F was subsequently carried out at 1000 °C in an argon atmosphere for 1 h; this sample is labeled as CN_x-FHT.

Powder samples (CN_x-P, CN_x-A, CN_x-F, CN_x-FHT) were characterized by scanning electron microscopy (SEM) (FEI Helios 600 Nanolab), Raman spectroscopy (HORIBA T6400, 633 nm and Reinshaw in Via Raman microscope, 514 and 785 nm), and X-ray powder diffraction (Bruker D8 DISCOVER with GADDS, with Cu Kα radiation, k = 1.54 Å). The powders were also dispersed ultrasonically in isopropyl alcohol in order to carry out transmission electron microscopy (TEM) studies (Cs corrector (2) equipped HR-TEM, JEM2100, JEOL, Japan). The samples were also characterized by scanning probe microscopy (SPM) (SII E-sweep) in the DFM mode. Samples for DFM were prepared on a silicon substrate from the ethanol suspensions using a dip coater. Powder samples (1 mg) were analyzed by thermal gravimetric analysis (Rigaku Thermo Plus TG8120) with a flow of air (300 cc/min) and a heating ramp of 10 °C/min. Surface chemical analysis was performed by X-ray photoelectron spectroscopy (XPS) using an Axis-Ultra (Kratos, UK). N_2 adsorption measurements were carried out for flake (CN_x-P) and buckypaper (CN_x-A and CN_x-F) samples at 77 K with a BELSORP-max, Bel Japan, Inc. Thermogravimetric mass spectrometry measurements were done with a skimmer-type differential thermobalance photoionization mass spectrometer simultaneous measurement system (Rigaku TG-DTA-PIMS 410/S) with a flow of He/O_2 (300 mL/min, O_2 at 19.82%), heating stage of 20 °C/min with an electron impact detector. Rapid heating in the presence of N_2 was made with a differential scanning calorimetry apparatus (Perkin-Elmer DSC 8500), from −70 to 280 K with heating ramps of 10 and 600 °C/min. Resistivity measurements of the different film samples were carried out using a Quantum Design physical properties measurement system (PPMS) from room temperature to 2 K.

Conflict of Interest: The authors declare no competing financial interest.

Acknowledgment. We acknowledge the support from the Program for Fostering Regional Innovation in Nagano from the Ministry of Education, Culture, Sports, Science and Technology of Japan. M.T., S.V.-D., F.T.-L., R.C.-S., and M.E. acknowledge support from the Research Center for Exotic Nanocarbons, Japan regional Innovation Strategy Program by the Excellence, JST. A.M.-G. acknowledges support from CONACYT for postdoctoral visit. B.G.S. was supported by the Center for Nanophase Materials Sciences, which is sponsored by the Office of Basic Energy Sciences at Oak Ridge National Laboratory, U.S. Department of Energy. Some of the calculations were performed using resources of the Oak Ridge Leadership Computing Facility and the National Center for Computational Sciences.

Supporting Information Available: Table of interlayer distances from XRD and I_D/I_G ratios from Raman spectroscopy. Table of atomic composition and functionalities obtained by XPS. Table of energy values for the insertion of a single N_2 molecule into triple-layer CNTs. Table of computed intercalation energies for different chemical species (nitrogen, sulfur dioxide, and trioxide, a sulfur atom, and hydrogen) and MWCNT defects (nitrogen substitutional, pyridine (N3), vacancy, and epoxy). Table of activation energies and resistivity values obtained with PPMS measurements. HRTEM images and TEM simulations of smooth edges of unzipped CN_x-MWNTs. DFM topography and line scans of V-shaped nanoribbon and amorphous-like nanoribbon. XRD and Raman spectroscopy of unzipped CN_x-MWNT. Thermogravimetric mass spectrometry and weight loss measurements of unzipped CN_x-MWNT. N_2 adsorption isotherms of unzipped CN_x-MWNT. Frames from the molecular dynamic simulations of the unzipping process of zigzag and defect zigzag nanotubes. Relaxed structures of SO_2 and SO_3 and charge distribution of SO_3, all intercalated within the outer walls of a triple wall CNT with an epoxy defect. Resistivity measurements of bulk film samples. Details for the DFT calculations. This material is available free of charge *via* the Internet at http://pubs.acs.org.

REFERENCES AND NOTES

1. Yakes, M. K.; Gunlycke, D.; Tedesco, J. L.; Campbell, P. M.; Myers-Ward, R. L.; Eddy, C. R., Jr.; Gaskill, D. K.; Sheehan, P. E.; Laracuente, A. R. Conductance Anisotropy in Epitaxial Graphene Sheets Generated by Substrate Interactions. *Nano Lett.* **2010**, *10*, 1559–1562.
2. Muñoz, E.; Lu, J.; Yakobson, B. I. Ballistic Thermal Conductance of Graphene Ribbons. *Nano Lett.* **2010**, *10*, 1652–1656.
3. Lee, C.; Wei, X.; Kysar, J. W.; Hone, J. Measurement of the Elastic Properties and Intrinsic Strength of Monolayer Graphene. *Science* **2008**, *321*, 385–388.
4. Li, X.; Wang, Zhang, X., L.; Lee, S.; Dai, H. Chemically Derived, Ultrasmooth Gaphene Nanoribbon Semiconductors. *Science* **2008**, *319*, 1229–1232.
5. Schedin, F.; Geim, A. K.; Morozov, S. V.; Hill, E. W.; Blake, P.; Katsnelson, M. I.; Novoselov, K. S. Detection of Individual Gas Molecules Adsorbed on Graphene. *Nat. Mater.* **2007**, *6*, 652–655.
6. Tapasztó, L.; Dobrik, G.; Lambin, P.; Biró, L. Tailoring the Atomic Structure of Graphene Nanoribbons by Scanning Tunnelling Microscope Lithography. *Nat. Nanotechnol.* **2008**, *3*, 397–401.
7. Elías, A. L.; Botello-Méndez, A. R; Meneses-Rodríguez, D.; González, V. J.; Ramírez-González, D.; Ci, L.; Muñoz-Sandoval, E.; Ajayan, P. M.; Humberto Terrones, H.; Mauricio Terrones, M. Longitudinal Cutting of Pure and Doped Carbon Nanotubes To Form Graphitic Nanoribbons Using Metal Clusters as Nanoscalpels. *Nano Lett.* **2010**, *10*, 366–372.
8. Campos-Delgado, J.; Romo-Herrera, J. M.; Jia, X.; Cullen, D. A.; Muramatsu, H.; Kim, Y. A.; Hayashi, T.; Ren, Z.; Smith, D. J.; Okuno, Y.; *et al.* Bulk Production of a New Form of sp^2 Carbon: Crystalline Graphene. *Nano Lett.* **2008**, *8*, 2773–2778.
9. Terrones, M. Materials Science: Nanotubes Unzipped. *Nature* **2009**, *458*, 845–846.
10. Kosynkin, D. V.; Higginbotham, A. L.; Sinitskii, A.; Lomeda, J. R.; Dimiev, A.; Price, B. K.; Tour, J. M. Longitudinal Unzipping of Carbon Nanotubes To Form Graphene Nanoribbons. *Nature* **2009**, *458*, 872–876.
11. Cano-Márquez, A. G.; Rodríguez-Macías, F. J.; Campos-Delgado, J.; Espinosa-González, C. G.; Tristán-López, F.; Ramírez-González, D.; Cullen, D. A.; Smith, D. J.; Terrones, M.; Vega-Cantu, Y. I. Ex-MWNTs: Graphene Sheets and Ribbons Prdocued by Lithium Intercalation and Exfoliation of Carbon Nanotubes. *Nano Lett.* **2009**, *9*, 1527–1533.
12. Jiao, L.; Zhang, L.; Wang, X.; Diankov, G.; Dai, H. Narrow Graphene Nanoribbons from Carbon Nanotubes. *Nature* **2009**, *458*, 877–880.
13. Datta, S. S.; Strachan, D. R.; Khamis, S. M.; Johnson, A. T. C. Crystallographic Etching of Few-Layer Graphene. *Nano Lett.* **2008**, *8*, 1912–1915.
14. Ci, L.; Xu, Z.; Wang, L.; Gao, W.; Ding, F.; Kelly, K. F.; Yakobson, B. I.; Ajayan, P. M. Controlled Nanocutting of Graphene. *Nano Res.* **2008**, *1*, 116.
15. Kim, K.; Sussman, A.; Zettl, A. Graphene Nanoribbons Obtained by Electrically Unwrapping Carbon Nanotubes. *ACS Nano* **2010**, *4*, 1362–1366.
16. Cai, J.; Ruffieux, P.; Jaafar, R.; Bieri, M.; Braun, T.; Blankenburg, S.; Muoth, M.; Seitsonen, A. P.; Saleh, M.; Feng, X.; *et al.* Atomically Precise Bottom-Up Fabrication of Graphene Nanoribbons. *Nature* **2010**, *466*, 470–473.
17. Jiao, L.; Wang, X.; Diankov, G; Wang, H.; Dai, H. Facile Synthesis of High-Quality Graphene Nanoribbons. *Nat. Nanotechnol.* **2011**, *5*, 321–325.
18. Tao, C.; Jiao, L.; Yazyev, O. V.; Chen, Y.-C.; Feng, J.; Zhang, X.; Capaz, R. B.; Tour, J. M.; Zettl, A.; Louie, S. G.; *et al.* Spatially Resolving Edge States of Chiral Graphene Nanoribbons. *Nat. Phys.* **2011**, *7*, 616–620.
19. Talyzin, A. V.; Luzan, S.; Anoshkin, I. V.; Nasibulin, A. G.; Jiang, H.; Kauppinen, E. I.; Mikoushkin, V. M.; Shnitov, V. V.; Marchenko, D. E.; Noréus, D. Hydrogenation, Purification, and Unzipping of Carbon Nanotubes by Reaction with Molecular Hydrogen: Road to Graphane Nanoribbons. *ACS Nano* **2011**, *5*, 5132–5140.
20. Paiva, M. C.; Xu, W.; Proença, M. F.; Novais, R. M.; Lægsgaard, E.; Besenbacher, F. Unzipping of Functionalized Multiwall Carbon Nanotubes Induced by STM. *Nano Lett.* **2010**, *10*, 1764–1768.
21. Jia, X.; Campos-Delgado, J.; Terrones, M.; Meunier, V.; Dresselhaus, M. S. Graphene Edges: A Review of Their Fabrication and Characterization. *Nanoscale* **2011**, *3*, 86–95.
22. Jia, X.; Hofmann, M.; Meunier, V.; Sumpter, B. G.; Campos-Delgado, J.; Romo-Herrera, J. M.; Son, H.; Hsieh, Y.-P.; Reina, A.; Kong, J.; *et al.* Controlled Formation of Sharp Zigzag and Armchair Edges in Graphitic Nanoribbons. *Science* **2009**, *323*, 1701–1705.
23. Kang, F.; Zhang, T.-Y.; Leng, Y. Electrochemical of Burn-Off on Thermal Shock Resistance of Nuclear Carbon Materials. *Carbon* **1997**, *35*, 1167–l173.
24. Toyodaa, M.; Katoha, H.; Shimizua, A.; Inagaki, M. Exfoliation of Nitric Acid Intercalated Carbon Fibers: Effect of Heat-Treatment Temperature of Pristine Carbon Fibers and Electrolyte Concentration on the Exfoliation Behavoir. *Carbon* **2003**, *41*, 731–738.
25. Nakajima, T.; Matsuo, Y. Formation Process and Structure of Graphite Oxide. *Carbon* **1994**, *32*, 469–475.
26. Shih, C.-J.; Vijayaraghavan, A.; Krishnan, R.; Sharma, R.; Han, J.-H.; Ham, M.-H.; Jin, Z.; Lin, S.; Paulus, G. L. C.; Reuel, N. F.; *et al.* Bi- and Trilayer Graphene Solutions. *Nat. Nanotechnol.* **2011**, *6*, 439–445.
27. Chen, G.; Weng, W.; Wu, D.; Wu, C. PMMA/Graphite Nanosheets Composite and Its Conducting Properties. *Eur. Polym. J.* **2003**, *39*, 2329–2335.
28. Dresselaus, M. S.; Dresselhaus, G. Intercalation Compounds of Graphite. *Adv. Phys.* **1981**, *30*, 139–326.
29. Chou, W.-J.; Wang, C.-C.; Chen, C.-Y. The Improvement of Electrical Property of Multiwalled Carbon Nanotubes with Plasma Modification and Chemical Oxidation in the Polymer Matrix. *J. Inorg. Organomet. Polym.* **2009**, *19*, 234–242.
30. Ago, H.; Kugler, T.; Cacialli, F.; Salaneck, W. R.; Shaffer, M. S. P.; Windle, A. H.; Friend, R. H. Work Functions and Surface Functional Groups of Multiwall Carbon Nanotubes. *J. Phys. Chem. B* **1999**, *103*, 8116–8121.
31. Kundu, S.; Wang, Y.; Xia, W.; Muhler, M. Thermal Stability and Reducibility of Oxygen-Containing Functional Groups on Multiwalled Carbon Nanotube Surfaces: A Quantitative High-Resolution XPS and TPD/TPR Study. *J. Phys. Chem. C* **2008**, *112*, 16869–16878.
32. Marcano, D.; Kosynkin, D. V; Berlin, J. M.; Sinitskii, A.; Sun, Z.; Slesarev, A.; Alemany, L. B.; Lu, W.; Tour, J. M. Improved Synthesis of Graphene Oxide. *ACS Nano* **2010**, *4*, 4806–4814.
33. Becerril, H. A.; Mao, J.; Liu, Z.; Stoltenberg, R. M.; Bao, Z.; Chen, Y. Evaluation of Solution-Processed Reduced Graphene Oxide Films as Transparent Conductors. *ACS Nano* **2008**, *2*, 463–470.
34. Higginbotham, A. L.; Kosynkin, D. V.; Sinitskii, A.; Sun, Z.; Tour, J. M. Lower-Defect Graphene Oxide Nanoribbons from Multiwalled Carbon Nanotubes. *ACS Nano* **2010**, *4*, 2059–2069.
35. Inoue, S.; Ichikuni, N.; Uematsu, T.; Kaneko, K. Capillary Condensation of N_2 on Multiwall Carbon Nanotubes. *J. Phys. Chem. B* **1998**, *102*, 4689–4692.
36. Li, Z.; Pan, Z.; Dai, S. Nitrogen Adsorption Characterization of Aligned Multiwalled Carbon Nanotubes and Their Acid Modification. *J. Colloid Interface Sci.* **2004**, *277*, 35–42.
37. Yanh, Q.-H.; Hou, P.-X.; Bai, S.; Wang, M.-Z.; Cheng, H.-M. Adsorption and Capillarity of Nitrogen in Aggregated Multi-Walled Carbon Nanotubes. *Chem. Phys. Lett.* **2001**, *345*, 18–24.
38. Stuart, S. J.; Tutein, A. B.; Harrison, J. A. A Reactive Potential for Hydrocarbons with Intermolecular Interactions. *J. Chem. Phys.* **2000**, *112*, 6472–6486.
39. Arora, G.; Wagner, N. J.; Sandler, S. I. Adsorption and Diffusion of Molecular Nitrogen in Single Wall Carbon Nanotubes. *Langmuir* **2004**, *20*, 6268–6277.

40. Li, S.-S.; Tu, K.-H.; Lin, C.-C.; Chen, C.-W.; Chhowalla, M. Solution-Processable Graphene Oxide as an Efficient Hole Transport Layer in Polymer Solar Cells. *ACS Nano* **2010**, *4*, 3169–3174.
41. Shklovskii, B. I.; Efros, A. L. Electonic Properties of Doped Semiconductors, In *Springer Series in Solid-State Sciences*; Springer: Berlin, 1984; Vol. 45.
42. Jang, W. Y.; Kulkarni, N. N.; Shih, C. K.; Yao, Z. Electrical Characterization of Individual Carbon Nanotubes Grown in Nanoporous Anodic Alumina. *Appl. Phys. Lett.* **2004**, *84*, 1177–1179.
43. Wang, D. P.; Feldmana, D. E.; Perkins, B. R.; Yin, A. J.; Wang, G. H.; Xu, J. M.; Zaslavsky, A. Hopping Conduction in Disordered Carbon Nanotubes. *Solid State Commun.* **2007**, *142*, 287–291.
44. Danneau, R.; Wu, F.; Tomi, M. Y.; Oostinga, J. B.; Morpurgo, A. F.; Hakonen, P. J. Shot Noise Suppression and Hopping Conduction in Graphene Nanoribbons. *Phys. Rev. B* **2010**, *82*, 161405.
45. Han, M. Y.; Brant, J. C.; Kim, P. Electron Transport in Disordered Graphene Nanoribbons. *Phys. Rev. Lett.* **2010**, *104*, 056801.
46. Gunlycke, D.; Areshkin, D. A; White, C. T. Semiconducting Graphene Nanostrips with Edge Disorder. *Appl. Phys. Lett.* **2007**, *90*, 142104.
47. Querlioz, D.; Apertet, Y.; Valentin, A.; Huet, K.; Bournel, A.; Galdin-Retailleau, S.; Dollfus, P. Suppression of the Orientation Effects on Bandgap in Graphene Nanoribbons in the Presence of Edge Disorder. *Appl. Phys. Lett.* **2008**, *92*, 042108.
48. Anderson, P. W. Absence of Diffusion in Certain Random Lattices. *Phys. Rev.* **1958**, *109*, 1492–1505.
49. Conway, N. M. J.; Ilie, A.; Robertson, J.; Milne, W. I.; Tagliaferro, A. Reduction in Defect Density by Annealing in Hydrogenated Tetrahedral Amorphous Carbon. *Appl. Phys. Lett.* **1998**, *73*, 2456–2458.
50. Veerasamy, V. S.; Yuan, J.; Amaratunga, G. A. J.; Milne, W. I.; Gilkes, K. W. R.; Weiler, M.; Brown, L. M. Nitrogen Doping of Highly Tetrahedral Amorphous Carbon. *Phys. Rev. B* **1993**, *48*, 17958–17959.
51. Wei, B.; Spolenak, R.; Kohler-Redlich, P.; Rühle, M.; Arzt, E. Electrical Transport in Pure and Boron-Doped Carbon Nanotubes. *Appl. Phys. Lett.* **1999**, *74*, 3149–3151.
52. Zahab, A.; Spina, L.; Poncharal, P.; Marliere, C. Water-Vapor Effect on the Electrical Conductivity of a Single-Walled Carbon Nanotube Mat. *Phys. Rev. B* **2000**, *62*, 10000–10003.
53. Terrones, M.; Kamalakaran, R.; Seeger, T.; Rühle, M. Novel Nanoscale Gas Containers: Encapsulation of N_2 in CN*x* Nanotubes. *Chem. Commun.* **2000**, 2335–2336.